Composites Communications 44 (2023) 101750

Contents lists available at ScienceDirect

Composites Communications

journal homepage: www.elsevier.com/locate/coco

Fine-tunable ε'-negative response derived from low-frequency plasma oscillation in graphene/polyaniline metacomposites

Yunpeng Qu [a], Qiong Peng [a,**], Yunlei Zhou [b,*], Farid Manshaii [c], Shaolei Wang [c], Kaidong Wang [c], Peitao Xie [d], Xiaosi Qi [a,***], Kai Sun [e]

[a] College of Physics, Guizhou University, Guiyang, 550025, China
[b] Hangzhou Institute of Technology, Xidian University, Hangzhou, 311231, China
[c] Department of Bioengineering, University of California, Los Angeles, Los Angeles, CA, 90095, USA
[d] College of Materials Science and Engineering, Qingdao University, Qingdao, 266071, China
[e] College of Ocean Science and Engineering, Shanghai Maritime University, Shanghai, 201306, China

A R T I C L E I N F O

Keywords:
Metacomposites
Polymer-matrix composites
Negative permittivity
ε'-near-zero

A B S T R A C T

Remarkable ε'-negative responses at radio-frequency endow metacomposites with revolutionary applications in electromagnetic (EM) fields. However, uncovering its regulation mechanism and subsequently achieving fine-tunable ε'-negative response remains challenging. Here, we meticulously designed graphene/polyaniline (GR/PANI) metacomposites above percolation, which directly enable tunable negative permittivity at an order of magnitude of -10^3. By rationally adjusting the three-dimensional GR network, we were able to form collective low-frequency plasma oscillation of free electrons in composites, which intrinsically contributes to the tunable ε'-negative response. Moreover, an ε'-near-zero (ENZ) response was surprisingly observed at ~920 MHz due to the ineffectiveness of the plasmonic state at high frequencies. In addition, we carried out equivalent circuit analysis to demonstrate the phase relationship and electrical characteristics of these metacomposites. This work could contribute to a new category of polymer-matrix composites and enable exotic properties beyond their natural and bulk counterparts.

1. Introduction

Recently, polymer-matrix composites (PMCs) have drawn considerable attention due to their superior physical parameters compared to those of each constituent material [1–3]. These improved properties have led to transformative applications in various scientific and industrial fields. The outstanding physical properties achieved by various PMCs have dramatically altered applications in fields such as electromagnetic (EM), thermal, dielectric, and mechanical fields, among others [1–5]. Particularly in relation to the EM media for manipulating EM waves, one innovative material system, metacomposites, a branch of EM metamaterials, was recently introduced and developed [6–9]. In this ever-expanding landscape, PMCs with negative parameters ($\varepsilon' < 0$ and/or $\mu' < 0$) have been considered as a new category of metacomposites, attracting significant research interest, especially in EM interface shielding, high-k capacitors, and next-generation electronic devices [10–12]. Benefiting from a significant correlation of the composition-structure-property in PMCs, metacomposites offer more design freedom in terms of chemical composition and microstructure [10–12]. This flexibility in design opens new possibilities for the optimization and application of these materials.

In the previous researches, attention has largely been focused on metal/ceramic metacomposites, such as those of Cu/TiO_2, Ni/TiO_2, $Cu/BaTiO_3$, $Ni/BaTiO_3$ and $Ag/CaCu_3Ti_4O_{12}$ composites [13–17]. By regulating the effective electron concentration (n_{eff}) of metacomposites, the otherwise meaningless complex permittivity ($\varepsilon = \varepsilon'$-$j\varepsilon''$) of mono-phase metals becomes effective at radio-frequency (MHz ~ GHz) band. This represents a significant shift in the operational bandwidth of these materials. That is, the plasmonic state of metals switches from the ultraviolet and visible light band to the radio-frequency region, allowing for the creation of novel EM and electronic devices based on metacomposites that could respond sensitively and effectively to millimeter

* Corresponding author.
** Corresponding author.
*** Corresponding author.
E-mail addresses: qpeng@gzu.edu.cn (Q. Peng), zhouyunlei@xidian.edu.cn (Y. Zhou), xsqi@gzu.edu.cn (X. Qi).

https://doi.org/10.1016/j.coco.2023.101750
Received 9 September 2023; Received in revised form 8 October 2023; Accepted 8 October 2023
Available online 10 October 2023
2452-2139/

and submillimeter EM waves [13–17].

Despite the significant achievements in metal/ceramic metacomposites, several issues, such as the chemical instability of nano-scale particles, high conduction loss, excessive relative density, and potential magnetic interference, have yet to be satisfactorily addressed [13–18]. Recently, research efforts have been devoted to carbon/polymer composites with negative permittivity, which aim to overcome the limitations of metallic fillers. Carbon nanomaterials such as carbon nanotube (CNT), graphene (GR), carbon black (CB), and carbon nanofiber (CNF) have gradually emerged as excellent alternatives for metallic fillers, due to their impressive physical parameters and chemical performance [19–23]. Unfortunately, the carbon/polymer metacomposites are experiencing the serious shortage of design principles and therefore suffer from the unclear regulation mechanism, which substantially restricts the development of polymer-based metacomposites.

Herein, different from the previous PANI-based metacomposites [1–3], we fabricated graphene/polyaniline (GR/PANI) metacomposites through aniline polymerization, ball-milling, and a high-pressure compression process. In doing so, three-dimensional (3D) conductive networks composed of two-dimensional (2D) GR sheets could meticulously constructed and adjusted. The negative permittivity value was successfully tuned at an order of magnitude of -10^3. This achievement was triggered by low-frequency collective plasma oscillation within the 3D carbon network. The GR/PANI metcomposites firstly earn fine-tunable ε'-negative responses and ENZ response at radio-frequency region which offer compelling avenues for further research and application in EM fields. Additionally, our obtained metacomposites provide a universal paradigm for PMCs, greatly enriching their design diversity and increasing the range of functionalities that can be achieved in the EM fields.

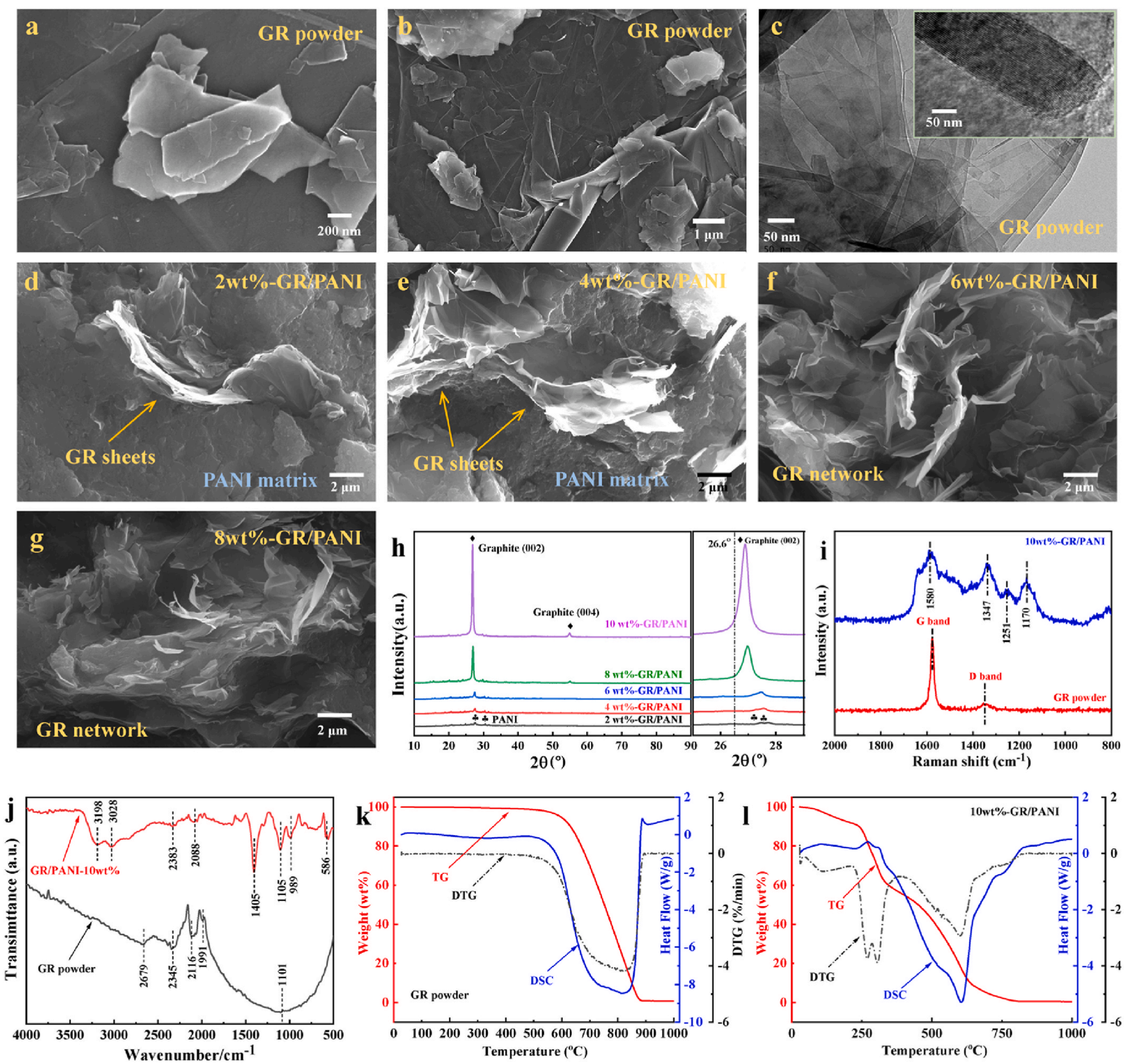

Fig. 1. SEM and TEM images (a–g), XRD patterns (h), Raman spectra (i), FT-IR spectra (j) and TG-DSC curves (k–l) of GR sheets and GR/PANI composites.

2. Results and discussion

2.1. Structural characterization

In what follows, we present a comprehensive analysis of the metacomposites, scrutinizing their structural, electrical, and functional properties. As displayed in Fig. 1a–g, the GR sheets display a typical 2D structure with a large conductive area, thereby greatly facilitating the formation of 3D networks. With an increase in GR content, the GR networks become increasingly prominent within GR/PANI metacomposites. By analyzing the XRD patterns of metacomposites in Fig. 1h, it is evident that no impure phase has been detected and the diffraction peaks of GR become gradually dominant with increasing GR content.

Subsequent analysis revealed several noteworthy points. The Raman spectra of GR sheets and 10 wt%-GR/PANI metacomposites, as illustrated in Fig. 1i, indicate their high degree of crystallization, as well as a certain level of structural defects in the metacomposites. Moreover, thanks to the physical preparation process of metacomposites, the multiple chemical bonds at the edge of GR sheets remain effective, as highlighted in Fig. 1j. The homogeneously ball-milling method protects GR and PANI raw materials from the damage of chemical agents such as acidic solution. Consequently, the excellent heat resistance of GR and GR/PANI metacomposites allows them to comply with real-world standards for electronic devices, as exhibited in Fig. 1k–i. This proves particularly valuable, as the materials retain their integrity until the temperature reaches around 600 °C for GR sheets and 250 °C for 10 wt %-GR/PANI metacomposites. It also inspires the future concerns on mechanical properties of metacomposites which could favor the practical applications on electronic devices.

2.2. Electrical properties

Having characterized the structural properties, we next examined the electrical properties of the metacomposites. As shown in Fig. 2a, the ac conductivity (σ_{ac}) displays a notable decreasing trend with frequency, echoing the metal-like conduction behavior commonly observed in similar metal-based composites [13–17]. Importantly, our fabricated metacomposites with a GR content of 2–10 wt% fall under the category of percolated composites, demonstrating already established 3D conductive networks.

The ensuing analysis explores the intricate relationship between electrical and material properties. In engineering parlance, metal-like conductivity is often accompanied by skin effects. The skin effect can be quantified by skin depth (δ) [13–17]:

$$\delta = \sqrt{\frac{2}{\omega\mu\sigma_{dc}}} \tag{1}$$

Here, ω represents the electric field frequency, σ_{ac} signifies dc conductivity, and μ stands for static permeability. This formula serves as a cornerstone for explaining our observations. The correlation between the skin effect and the noticeable decrease in σ_{ac} at high frequencies is elucidated by employing the tendency of decreasing δ. According to the original design paradigm of GR/PANI metacomposites, a ε'-negative response could be achieved in the percolated state of composites when 3D GR networks are efficiently integrated into the PANI matrix. In this way, the interfacial polarization between GR and PANI is no longer the primary dielectric response mechanism. As illustrated in Fig. 2b, all samples demonstrate negative permittivity ($\varepsilon' < 0$) across all test frequencies, except for the 6 wt%-GR/PANI metacomposites. This exception prompts further investigation into compositional or structural differences. The absolute values of ε' increase with the increase in GR content, which can be attributed to the enhanced low-frequency collective plasma oscillation within the 3D carbon networks, as outlined in Fig. 4. The dashed lines in Fig. 2b serve as fitting results for GR/PANI metacomposites using the Drude model [8,9]:

$$\varepsilon' = \varepsilon_{\infty} - \frac{\omega_p^2}{\omega^2 + \Gamma_D^2} \tag{2}$$

$$\omega_p = \sqrt{\frac{ne^2}{m\varepsilon_0}} \tag{3}$$

where ε_{∞} means optical permittivity ($\omega \rightarrow \infty$) and Γ_D indicates the damping factor. The parameters in the equations are crucial for tuning the electrical characteristics of the composites. The ω_p is plasma frequency which is determined by effective electron density n and electron

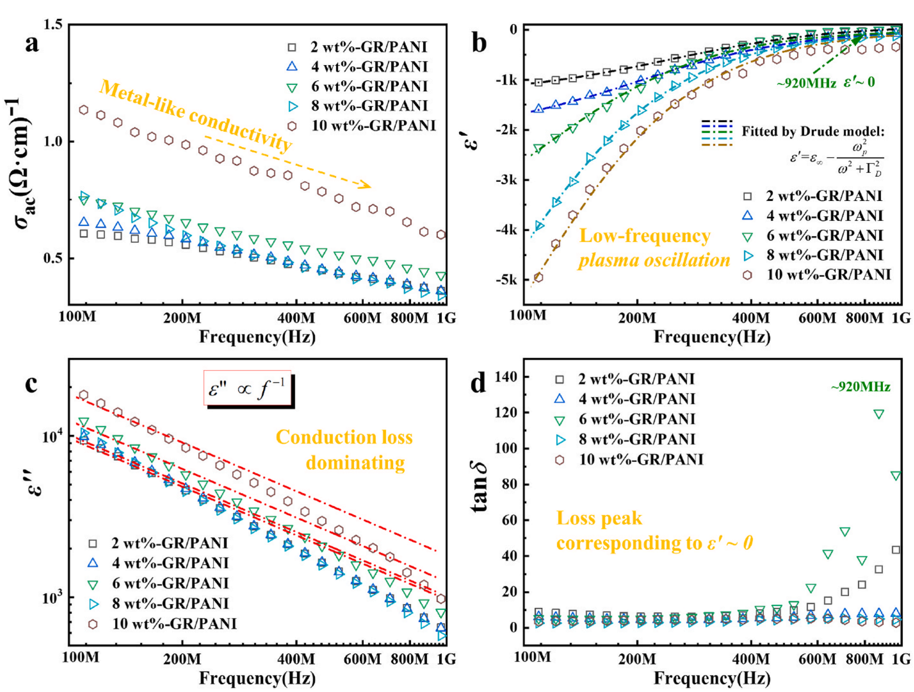

Fig. 2. Frequency-dependent measurements of ac conductivity (a), complex permittivity (b–c), and loss tangent angle (d) for GR/PANI composites.

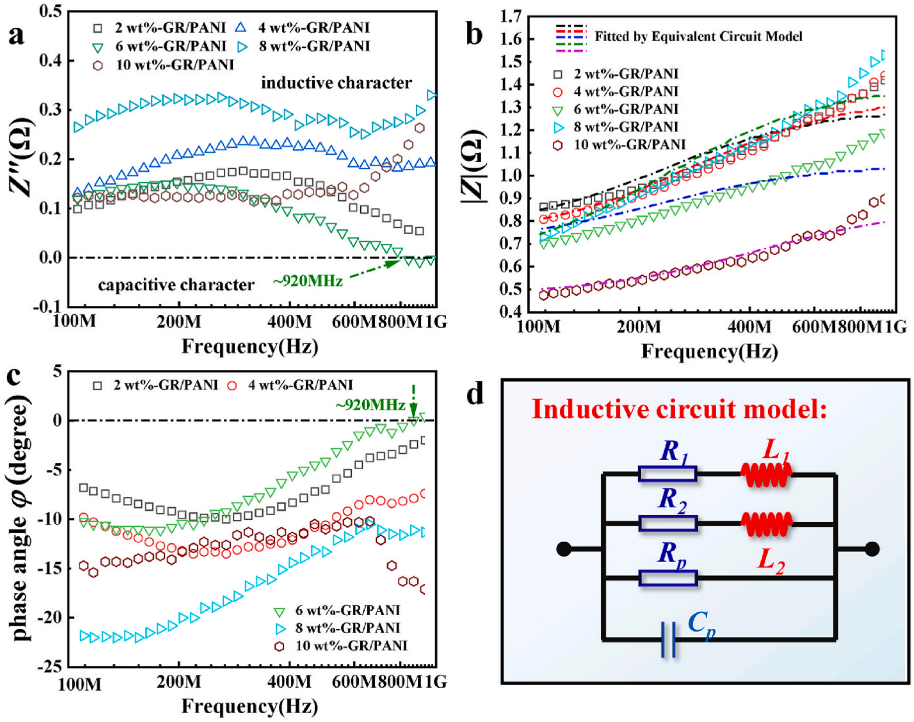

Fig. 3. Frequency dispersions of reactance (a), impedance modulus (b), and phase angle (c) for GR/PANI composites. The dashed lines in (b) are fitting results from equivalent circuit models as shown in (d).

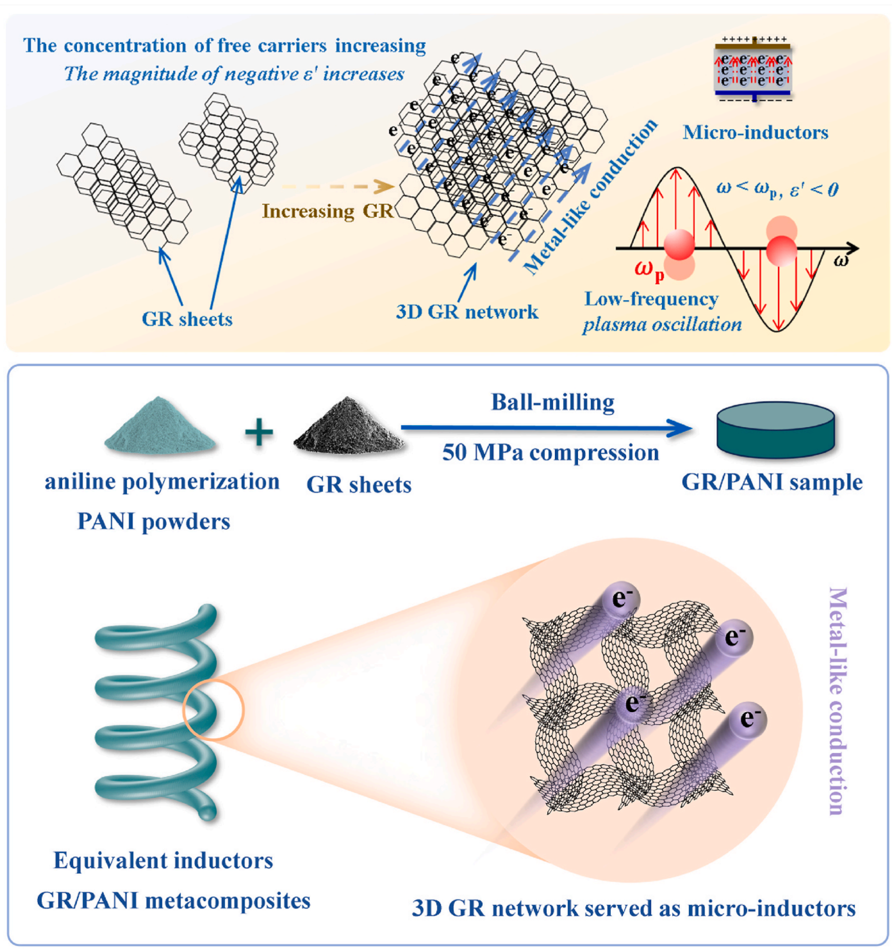

Fig. 4. Schematic diagram illustrating the generation mechanism of ε'-negative response with microstructural evolution.

weight m. The low-frequency plasma oscillation, colloquially known as plasmonic state, is directly related to the concentration of free electrons in 3D GR networks. This relationship explains the steady rise in the negative value of ε' from approximately 1000 to around 5000 at nearly 100 MHz. In essence, the GR sheets serve not only as microstructural components in the PANI matrix but also contribute to the free carriers of the plasma state. Besides, the semiconductive PANI matrix facilitated the fine-tunable ε'-negative response by contributing to the regulation of plasma oscillation. A noteworthy observation is the ε'-near-zero (ENZ) response at about 920 MHz in 6 wt%-GR/PANI metacomposites, which correlates with its concentration of free carriers. This phenomenon indicates a shift in the plasma oscillation frequency in relation to the incident electrical field. In fact, the ε'-negative response occurs when the plasma oscillation frequency is larger than the incident electrical field frequency ($\omega_p > \omega$), as schematically shown in Fig. 4. With the formation of 3D conductive GR networks in metacomposites, dielectric loss inevitably grows, as indicated in Fig. 2c. The imaginary permittivity (ε'') shows a decreasing trend with frequency, suggesting the predominance of conduction loss (ε_c'') in composites. The dash lines are the fitting results of ε_c'' which presents its principal part and the minor division of relaxation loss (ε_r''), This obvious disparity to the experimental data at high frequencies was due to the change of conduction mechanism. As shown in loss tangent ($\tan\delta = |\varepsilon''/\varepsilon'|$) spectra (Fig. 2d), there is a loss peak at approximately 920 MHz, which directly correlates to the ENZ behavior in 6 wt%-GR/PANI metacomposites. This implies that there could be significant energy fluctuation around the ENZ frequency when plasma oscillation ceases down at higher frequencies, making this material intriguing for applications requiring precise frequency response.

2.3. Equivalent circuit analysis

Building off the analysis of electrical properties, we further performed equivalent circuit analysis to model the impedance response. There is an inherent relationship between reactance Z'' and ε' for ε'-negative materials [14,15]:

$$\varepsilon' = -\frac{Z''}{\omega C_0 \left(Z'^2 + Z''^2\right)} \tag{4}$$

where C_0 is vacuum capacitance, Z' means resistance. In Fig. 3a, the metacomposites display a uniformly positive value of Z'' across all test frequencies, except for the 6 wt%-GR/PANI metacomposites, indicating an inductive character. This observation provides a new direction for studying inductive components like coil-less inductors and laminated capacitors. It's critical to note that the character changes from inductive to capacitive with increasing frequency across the ENZ frequency in 6 wt%-GR/PANI metacomposites, suggesting a Z''-near-zero behavior. The equivalent circuit model for impedance modulus spectra ($|Z|$), presented in Fig. 3b–d, reveals varying intrinsic inductive character and current-voltage phase relationships compared to conventional dielectrics. The $|Z|$ increases with the incremental electric field frequency, which corresponds to the skin effect of metacomposites, as schematic in Fig. 4. The output data of inductive circuit model show mismatching tendency because of the no longer ineffective plasma oscillation at high frequencies (Fig. 3b). The inductive character originates from the 3D GR networks, which could be equivalent to millions of micro-inductors. The phase angle (θ) values are consistently positive, indicating a lag in the current phase relative to the voltage phase. For ENZ materials, however, this lag is minimized, indicating near-pure resistance. In conclusion, the ε'-negative and ENZ media exhibit inductive properties, which hold promise for applications such as advanced EM shielding, innovative coil-less inductors, and next-generation electronic devices [4,18,24–26].

3. Conclusion

Herein, the resulting GR/PANI metacomposites achieved tunable negative permittivity at an order of magnitude of -10^3. Low-frequency collective plasma oscillations of free electrons were realized in the metacomposites, which initiate a Drude-type ε'-negative response. The resultant ENZ response at approximately 920 MHz stems from the inactivity of the plasmonic state when the plasma frequency is lower than the external electric field frequency. This work serves as a foundational study for achieving finely-tunable ε'-negative responses and has the potential to significantly broaden the scope of PMCs and their real-world applications in the electromagnetic field.

CRediT authorship contribution statement

Yunpeng Qu: Conceptualization, Methodology, Writing – review & editing. **Qiong Peng:** Conceptualization, Methodology, Writing – review & editing. **Yunlei Zhou:** Conceptualization, Methodology, Writing – review & editing. **Farid Manshaii:** Data curation, Reviewing, Supervision. **Shaolei Wang:** Data curation, Reviewing, Supervision. **Kaidong Wang:** Data curation, Reviewing, Supervision. **Peitao Xie:** Reviewing, Supervision. **Xiaosi Qi:** Reviewing, Supervision. **Kai Sun:** Reviewing, Supervision.

Declaration of competing interest

The authors declare that they have no known competing financial interests or personal relationships that could have appeared to influence the work reported in this paper.

Data availability

Data will be made available on request.

Acknowledgements

This work was supported by the National Natural Science Foundation of China (Grant No. 52205593), the Fund of Natural Science Special (Special Post) Research Foundation of Guizhou University (Grant No. 2023–032), and Platform of Science and Technology and Talent Team Plan of Guizhou province (GCC [2023] 007).

References

[1] K. Sun, W. Duan, et al., Composer Part a-Appl S 156 (2022), 106854.
[2] Y. Zhou, Y. Qu, et al., Compos. Sci. Technol. 223 (2022), 109415.
[3] Y. Qu, Z. Wang, et al., Compos. Sci. Technol. 217 (2022), 109092.
[4] X. Tang, Z. Zhang, et al., Eng. Sci. 24 (2023) 920.
[5] H. Cai, Z. Qian, et al., Compos. Commun. 43 (2023), 101700.
[6] C. Deng, Y. Wu, et al., Compos. Commun. 43 (2023), 101724.
[7] Y. Qu, H. Wu, et al., Rare Met. (2023), https://doi.org/10.1007/s12598-023-02346-5.
[8] D. Smith, J. Padilla, et al., Phys. Rev. Lett. 84 (2000) 4184–4187.
[9] D. Schurig, J. Mock, et al., Science 314 (2006) 977–980.
[10] C. Cheng, Y. Liu, et al., Composer Part a-Appl S 155 (2022), 106842.
[11] L. Sun, Z. Shi, et al., Adv. Funct. Mater. 31 (2021), 2100280.
[12] J. Chen, G. Qin, et al., Org. Electron. 104 (2022), 106470.
[13] Z. Wang, K. Sun, et al., Acta Mater. 185 (2020) 412–419.
[14] G. Fan, Z. Wang, et al., Compos. Commun. 24 (2021), 100667.
[15] G. Fan, Z. Wang, et al., Scripta Mater. 190 (2021) 1–6.
[16] Z. Wang, K. Sun, et al., J. Materiomics. 6 (2020) 145–151.
[17] Y. Qu, J. Wu, et al., Scripta Mater. 203 (2021), 114067.
[18] Z. Wei, Z. Wang, et al., J. Mater. Sci. Technol. 112 (2022) 77–84.
[19] C. Cheng, Y. Wu, et al., Ceram. Int. 46 (2020) 2261–2267.
[20] Y. Qu, Y. Wu, et al., J. Alloys Compd. 847 (2020), 156526.
[21] Y. Liu, C. Cheng, et al., Composer Part a-Appl S 173 (2023), 107660.
[22] Y. Qu, Y. Wu, et al., J. Alloys Compd. 847 (2020), 156526.
[23] C. Deng, Y. Li, et al., Ceram. Int. 49 (2023) 16149–16155.
[24] S. Wang, Y. Nie, et al., Sci. Adv. 8 (2022), eabl5511.
[25] Y. Li, T. Fang, et al., Proc. Natl. Acad. Sci. U.S.A. 120 (2023), e2300953120.
[26] Y. Qu, P. Xie, et al., Ceram. Int. (2023), https://doi.org/10.1016/j.ceramint.2023.09.066.